Simple Acridan-Based Multi-Resonance Structures Enable Highly-Efficient Narrowband Green TADF Electroluminescence

Pengcheng Jiang,[a,b,+] *Lisi Zhan,*[c,+] *Xiaosong Cao,*[a,*] *Xialei Lv,*[a] *Shaolong Gong,*[c,d,*] *Changjiang Zhou,*[a] *Zhongyan Huang,*[a] *Fan Ni,*[a] *Yang Zou,*[a] *Chuluo Yang* [a,c,*]

[a] Shenzhen Key Laboratory of Polymer Science and Technology, College of Materials Science and Engineering, Shenzhen University, Shenzhen 518060, People's Republic of China

E-mail: xcao@szu.edu.cn (X.C.); clyang@szu.edu.cn (C.Y.)

[b] College of Physical and Optoelectronic Engineering, Shenzhen University, Shenzhen 518060, People's Republic of China

[c] Hubei Key Lab on Organic and Polymeric Optoelectronic Materials, Department of Chemistry, Wuhan University, Wuhan, 430072, People's Republic of China

Email: slgong@whu.edu.cn (S.G.)

[d] Shenzhen Research Institute of Wuhan University, Shenzhen 518057, People's Republic of China

[+] These authors contributed equally to this work.

Abstract

Multi-resonance thermally activated delayed fluorescence (MR-TADF) offered exceptional solution for narrowband organic light emitting diode (OLED) devices in terms of color purity and luminescence efficiency, while the development of new MR skeleton remained an exigent task, especially for long wavelength region. We hereby demonstrate that a simple modification of the B (boron)-N (nitrogen) framework by sp^3-carbon insertion would significant bathochromic shift the short-range charge-transfer emission and improve the device performances. The bis(acridan)phenylene-based skeleton developed in this contribution presented a non-planar conformation and allowed facile introduction of isolating units to prevent triplet-involved quenching, deriving two luminophores with quantum yields approaching 90% and narrow FWMHs below 30 nm in film state. Corresponding green-emissive devices realized superior performances comparing to the planar carbazolyl-based MR-TADF analogues, with a maximum external quantum efficiency (EQE_{max}) up to 28.2% and small efficiency roll-off without the involvement of any sensitizing host.

Purely organic thermally activated delayed fluorescence (TADF) emitters have proved effective in the use of organic light emitting diodes (OLEDs) due to their low production-cost as well as the capability to harvest "dark" triplet excitons *via* a reverse intersystem crossing (RISC) mechanism.[1-4] Facilitating of RISC is made by reduction of the energy gap (ΔE_{ST}) between the lowest excited singlet and triplet (S_1 and T_1) states, typically achieved in twisted donor-acceptor (D-A) typed molecules with separated frontier molecular orbitals (FMOs) at the expense of low oscillator strength (*f*) and photoluminescence quantum yield (Φ_{PL}).[5-8] This contradiction undoubtedfully sets an obstacle to obtain highly efficient emitter, and the large structural reorganization occurred in the excited state would cause broad emission spectra and increased non-radiative decay channels, eventually weakening the performances of corresponding devices.[9-15]

Instead of the conventional D-A configured emitters, a unique category of multi-resonance TADF (MR-TADF) molecules based on fused polycyclic aromatics was lately proposed by Hatakeyama et. al. to mitigate the aforementioned issues.[16-21] The complementary resonance effects of electron-deficient B and electron-rich N/O atoms within the framework separates the FMOs to induce short-range charge-transfer (SR-CT), concurrently offering small ΔE_{ST} and high radiative decay rate (10^7~10^8 s^{-1}) from S_1 to ground state (S_0).[17, 22] The planar nature with high rigidity guaranteed narrow full width at half maximum (FWHM) emissions, and could also induce favorable horizontal dipole orientation of the emitters to boost optical out-coupling efficiency. Thus far, the majority of the blue MR-TADF emitters were constructed from the basic motif DABNA

(Scheme 1) due to synthetic feasibility and their decent quantum efficiencies.[23] Replacement of the diphenylamino subunits into carbazolyl derived BN-CZ as a new core skeleton with bathochromic emission, which was adopted to realize full-color electroluminescence (EL) with high color purity and maximum external quantum efficiencies (EQE_{max}s) above 20% by peripheral electronic modulation.[24-28] Nonetheless, most MR-TADF devices encountered severe triplet-related efficiency loss at high luminance/current density due to aggregation-caused quenching (ACQ) stemmed from the intrinsic structural planarity and long delayed lifetime, and relied on the involvement of sensitizing host to avoid triplet accumulation.[29-31] Further, the structural diversity and scope of these emitters were still rather limited.[32] In this context, it remains an imperative and important task to develop novel MR-TADF fluorophores to fulfill satisfactory EQE, small efficiency roll-off, and pure emission color in devices.

Herein, a new series of MR-TADF emitters employing the simple bis(acridan)phenylene skeleton, with a collective name of **BN-AC**, was proposed and demonstrated as excellent candidates for green-emissive devices possessing concurrent EL and decent color purity (Fig. 1). The skeleton differed from DABNA with the insertion of two sp^3 carbon atoms, which served as locks to rigidify the molecular backbone, and also imposed significant impact on the corresponding photophysical properties by extending the FMO to the appended phenyl units. In addition, the presence of non-conjugated sp^3-linkage allowed facile introduction of peripherals that could inhibit the notorious bimolecular interaction. Alternation of the substituents to bulkier

ones could enhance the Φ_{PL} in solid-state and eventually lead to high EQE (approaching 30%) and greatly relieved roll-off character in devices.

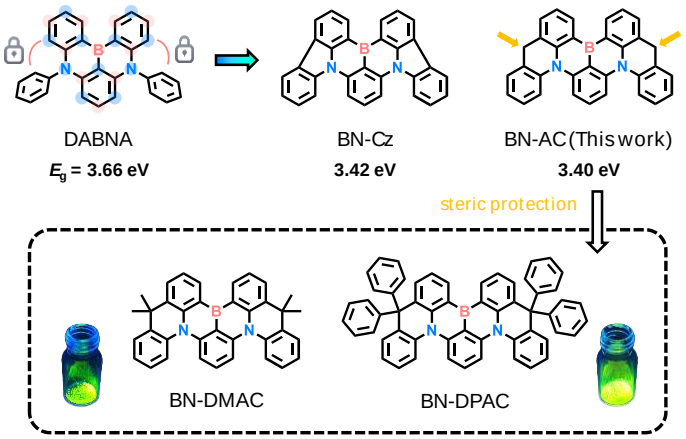

Scheme 1. The molecular design strategy and chemical structures of the green acridan-based MR-TADF emitters.

Density functional theory (DFT) and time-dependent DFT (TD-DFT) calculations at the B3LYP/6-31G(d,p) level were conducted to estimate the effect of structural variation on optoelectronic properties. Resulted from the tilted phenyl units that delocalized the FMO distribution and hyper-conjugation effect of sp^3 linkage, the **BN-AC** possessed a drastically reduced bandgap of 3.40 eV comparing to that of DABNA (3.66 eV), even narrower than BN-Cz (3.42 eV). Since the sp^3-carbon insertion showed no adverse effect to the multi-resonance, the current skeleton would be suitable for construction of highly efficient luminophores with green or even longer wavelength emission, considering its poorer core planarity than the carbazolyl analogue to weaken the ACQ effect. To investigate the influence of steric protection on **BN-AC** framework, methyl and phenyl substituted fluorophores, namely **BN-DMAC** and **BN-DPAC**, were

designed. For both compounds, the opposing resonance effects of N and B atom effectively separated the FMO distributions, consequentially leading to suitable ΔE_{ST}s yet preserving substantial $S_1 \rightarrow S_0$ oscillation strengths (*f*s) of 0.2914 and 0.3340 for **BN-DMAC** and **BN-DPAC**, respectively, noting the *f* for DABNA was only 0.2046 (Fig. 1A). The causes of larger *f* value and slightly narrower bandgap observed in **BN-DPAC** (3.38 eV compared with 3.41 eV of **BN-DMAC**) were due to the presence of additional homo-conjugation effect. The triplet spin-density distributions (SDD) resided on the whole multi-resonance skeleton except for the appended substituents on sp^3-hybridized carbon of the acridan subunits, clearly reflecting their insulating character to weaken the undesirable electron-exchange interactions. In addition, the small $S_1 \leftarrow S_0$ geometry changes of both compounds, as reflected by the root-mean-square displacement (RMSD) values during the excitation process (0.064 Å for **BN-DMAC** and 0.069 Å for **BN-DPAC**, Fig. 1B), hinted limited vibrational relaxation at S_1 and thereby the radiative-less internal conversion could be mitigated.[33]

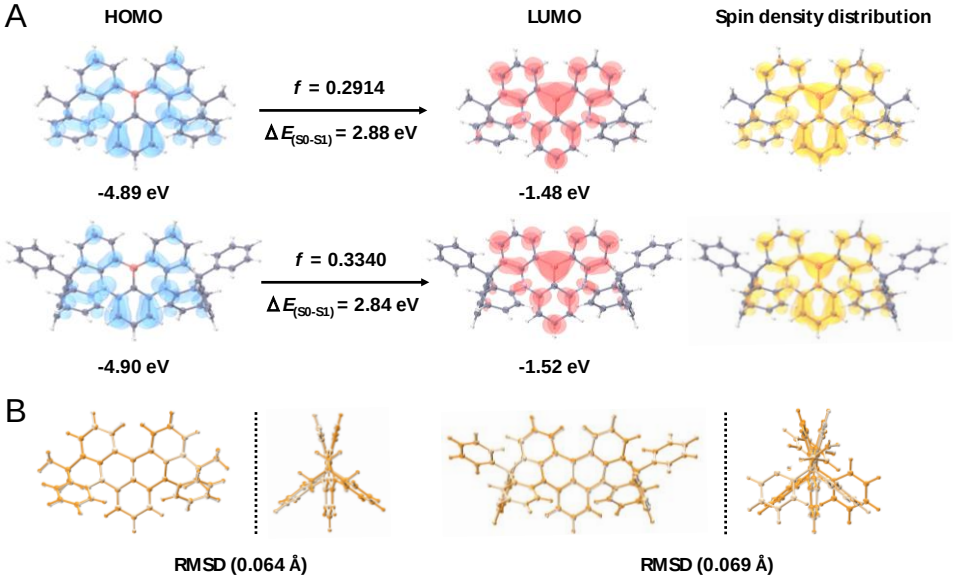

Figure 1. (A) Molecular conformations, distributions of frontier molecular orbitals (left) and triplet spin density distribution (right) of **BN-DMAC** and **BN-DPAC**. (B) Comparison of the S_0 (white) and S_1 (orange) structures.

BN-DMAC and **BN-DPAC** were acquired through a two-step synthetic procedure, including Buchwald amination to form the halogenated intermediates, and subsequent one-pot borylation (see Supporting Information for details). As the dangling substituents on acridan subunits would inevitably affect intermolecular interactions,[34-35] single crystals were cultured by slow evaporation of the ethanol/dichloromethane mixed solution. The X-ray crystallography indicated helical conformations for both compounds due to the presence of multiple sterically crowded hetero[4]helicenes, with large dihedral angles >30° between C and C' planes, and >50° between A and D/D' planes. As illustrated in Fig. 2A, the monoclinic **BN-DMAC** crystal featured distinct π-stacked substructures between adjacent B-N-containing skeletons, with a density of 1.282 g cm^{-3} and a centroid-centroid separation of 6.432 Å within dimeric species. Nevertheless, the π-π contact with a minimal distance of 3.713 Å was still weaker than many of the planar π-conjugated BN-Cz derivatives. In sharp comparison, the density of triclinic **BN-DPAC** crystal was merely 1.140 g cm^{-3}, suggesting very loose stacking modes with significant elongated centroid-centroid distance to 10.327 Å (Fig. 2B). The π-π stacking occurred only at the dummy peripheries with a complete isolation of the phenyl embraced B-N core, and such pseudo-dimeric packing patterns would be beneficial for quenching suppression.

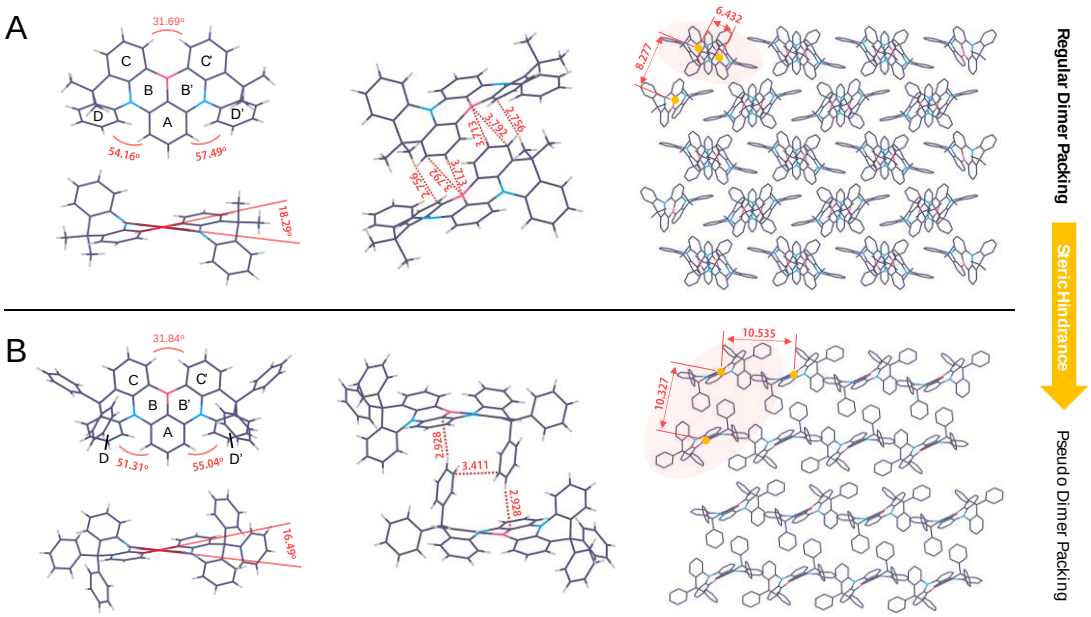

Figure 2. Single crystal information and packing diagram of (A) **BN-DMAC** (CCDC: 2044547); (B) **BN-DPAC** (CCDC: 2044549).

The emitters possessed strong intramolecular SR-CT absorption bands at 460 and 465 nm in dilute toluene solutions (1×10^{-5} M), and displayed structureless $S_0 \leftarrow S_1$ emission bands with peak wavelengths at 485 and 490 nm for **BN-DMAC** and **BN-DPAC**, respectively (Fig. 3A). Their multi-resonance structures with weak geometry relaxation resulted in small Stokes shifts below 25 nm and FWHMs smaller than 30 nm. The ΔE_{ST} values were deduced to be 0.14 eV for **BN-DMAC** and 0.11 eV for **BN-DPAC** based on the onset of the fluorescence and phosphorescence spectra (recorded at 77 K), promising efficient exciton upconversion avenue at ambient temperature. By varying the polarity of solvents from hexane to dichloromethane, positive solvatochromic effect with more pronounced bathochromic shifts (ca. 20 nm) and

broadened FWHMs was noticed comparing to the blue MR-TADF emitters, in accordance with the more delocalized FMOs (Fig. S1).

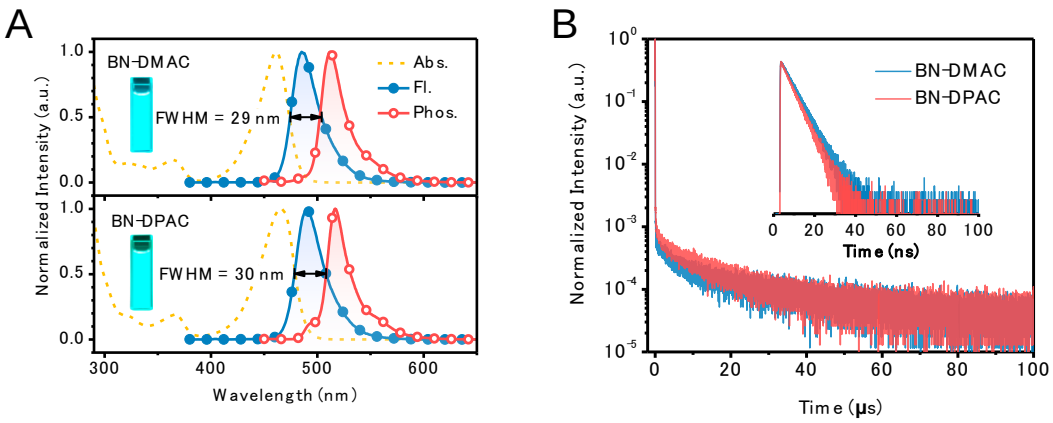

Figure 3. (A) UV-visible absorption (Abs.), Steady state fluorescence (Fl., measured at 300 K) and time-resolved phosphorescence (Phos., measured at 77 K) spectra of **BN-DMAC** and **BN-DPAC** in toluene (1×10^{-5} M); (B) transient photoluminescence decay curves of 1 wt% emitters in mCBP thin films under inert atmosphere.

The TADF profiles were testified in film state thereafter (Fig. 3B) by selecting 3,3'-di(9*H*-carbazol-9-yl)-1,1'-biphenyl (mCBP) as the host matrix in virtue of its high-lying T_1 to prevent energy back-transfer and appropriate FMO levels. Transient PL measurements clearly indicated the participation of triplet excited states in the emission mechanism, with the prompt and delayed fluorescence lifetimes (τ_{PF}, τ_{DF}) determined to be 5.1 ns, 13.9 μs and 4.4 ns, 11.6 μs for **BN-DMAC** and **BN-DPAC**, respectively. **BN-DPAC** manifested higher Φ_{PL} of 0.86 and more significant contribution from the DF component (η_{DF} = 0.32) comparative to the methyl substituted counterpart (Φ_{PL} = 0.63, η_{DF} = 0.25). The radiative and non-radiative decay rate constants of S_1 ($k_{r,S}$ and

$k_{nr,S}$) and reverse intersystem crossing (k_{RISC}) were next deduced to provide a more intuitive comparison between the two emitters (Table 1), where **BN-DPAC** was superior in nearly every aspects in consistence with its higher *f*, smaller ΔE_{ST}, and rigid structure enveloped with bulky periphery. Remarkably, the k_{RISC} values for both compounds surpassed most MR-TADF emitters, *e.g.* two magnitudes higher than DABNA (9.9×10^3 s^{-1}) recorded at the same condition, indicating efficient triplet-harvesting that might involve upper excited states (Table S1).[9, 21, 24] These represented promising characteristics of TADF dye for fabricating OLED with high performance.

Table 1. Summary of photophysical properties.

Emitter	λ_{abs} [a] (nm)	λ_{em} [a] (nm)	λ_{ph} [a] (nm)	FWHM [a] (nm)	ΔE_{ST} [a] (eV)	Φ_{PL} [b] (%)	τ_{PF} [b] (ns)	τ_{DF} [b] (μs)	$k_{r,S}$ [b] (10^8 s^{-1})	$k_{nr,S}$ [b] (10^7 s^{-1})	k_{ISC} [b] (10^7 s^{-1})	k_{RISC} [b] (10^5 s^{-1})
BN-DMAC	461	485	512	29	0.14	63	5.1	13.9	0.92	5.44	4.86	0.96
BN-DPAC	465	490	516	30	0.11	86	4.4	11.6	1.30	2.31	7.21	1.26

[a] Maximum wavelength of UV absorption (λ_{abs}), fluorescence (λ_{em}, 300 K), phosphorescence (λ_{ph}, 77 K), full-width at half-maximum (FWHM) and S_1-T_1 energy gap (ΔE_{ST}) measured in 1×10^{-5} M toluene solution; [b] absolute photoluminescence quantum yield (Φ_{PL}), as well as rate constants of singlet radiative decay ($k_{r,S}$), non-radiative decay ($k_{nr,S}$), intersystem crossing (k_{ISC}), reverse intersystem crossing (k_{RISC}) measured in 1 wt%-doped films of emitters in mCBP.

The high decomposition temperatures (T_ds, at 5 wt% loss) at 377 °C for **BN-DMAC** and 418 °C for **BN-DPAC** made these compounds suitable for device fabrication *via* vacuum-deposition process (Fig. S2). The **BN-AC** typed molecules were subsequently explored as the green fluorescent emitters in OLEDs, with architecture of indium tin oxide (ITO)/1,4,5,8,9,11-hexaazatriphenylene hexacarbonitrile (HAT-CN) (5 nm)/1,1-bis[(di-4-tolylamino)phenyl]cyclohexane (TAPC) (30 nm)/3-bis(9*H*-carbazol-9-yl)benzene (mCP) (10 nm)/1 wt% emitter in mCBP (20 nm)/(1,3,5-triazine-

2,4,6-triyl) tris(benzene-3,1-diyl) tris(diphenylphosphine oxide) (PO-T2T) (10 nm)/1,3,5-tri(*m*-pyrid-3-yl-phenyl)benzene (TmPyPB) (40 nm)/8-hydroxyquinolinato lithium (Liq) (1.5 nm)/aluminum (Al) (100 nm), where HAT-CN, TAPC, mCP, mCBP, PO-T2T, TmPyPB, Liq served as hole-injection, hole-transporting, electron-blocking, host, hole-blocking, electron-transporting and electron-injection materials, respectively. The emitting layer (EML) was sandwiched between two exciton-blocking layers for exciton-confinement. The corresponding energy level diagrams of devices and chemical structures were listed in Fig. 4A and Scheme S1.

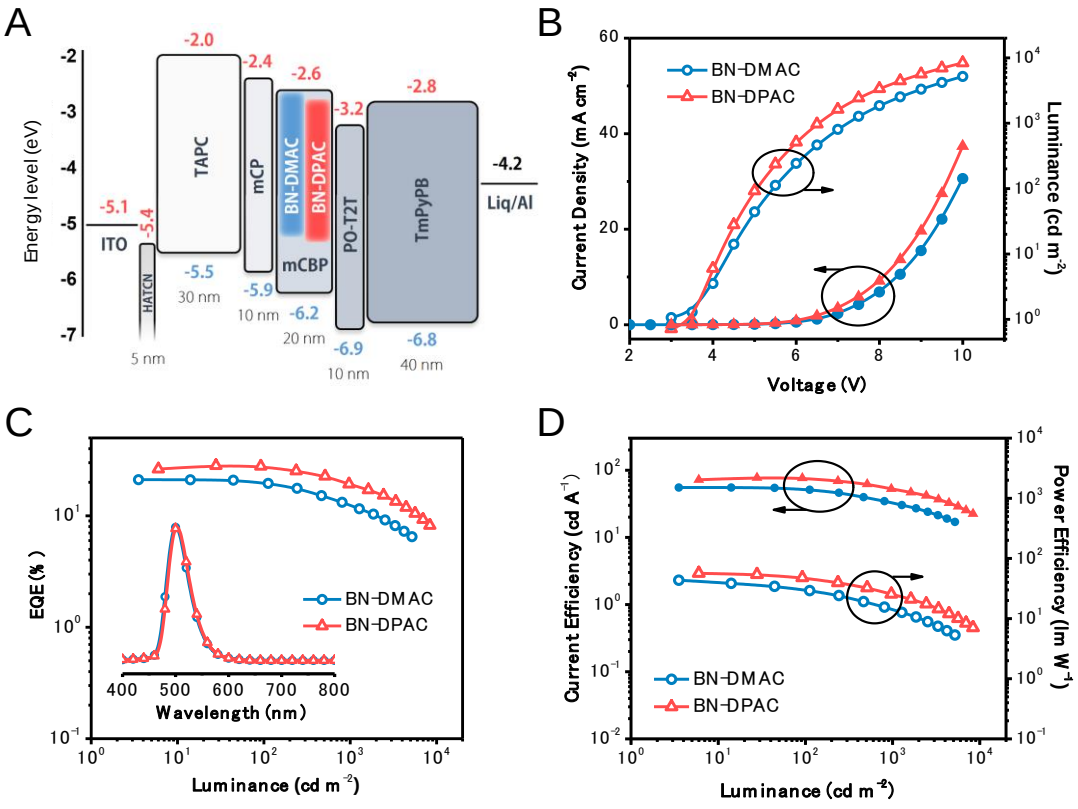

Figure 4. (A) Device architecture for the MR-TADF OLEDs with energy level alignment of the relevant materials; (B) current density and luminance versus voltage (*J-V-L*) characteristics; (C) external quantum efficiency (EQE)-luminance curves with

normalized electroluminescence (EL) spectra as the inset; (D) current efficiency (CE) and power efficiency (PE) versus luminance.

Table 2. Summary of the electroluminescence data.

Emitter	x (wt%)	V_{on}[a] (V)	CE_{max}[b] (cd A^{-1})	PE_{max}[c] (lm W^{-1})	EQE[d] (%)	λ_{EL}[e] (nm)	FWHM[f] (nm)	CIE[g] (x, y)
BN-DMAC	1	3.0	55.2	43.4	21.1/19.7/12.5	502	48	0.14, 0.54
BN-DPAC	1	3.5	77.3	56.5	28.2/27.7/19.2	504	48	0.14, 0.56
BN-DPAC	5	3.0	80.5	63.2	23.5/21.6/16.3	516	50	0.21, 0.65
BN-DPAC	10	3.0	75.5	58.6	21.4/21.1/16.3	518	50	0.22, 0.65

[a] Turn-on voltage at 1 cd m^{-2}; [b] maximum current efficiency; [c] maximum power efficiency; [d] external quantum efficiency: maximum, values at 100, 1000 cd m^{-2}; [e] emission peak of device; [f] full-width at half-maximum; [g] Commission Internationale de l'Eclairage coordinates.

The suitable energy cascade between functional layers as well as ideal charge carrier injection of the emitter ensured relatively low turn-on voltages (V_{on}, at 1 cd m^{-2}) below 3.5 V for both devices (Fig. 4B). The EL characteristics indicated green emission at 502 nm for **BN-DMAC** and 504 nm for **BN-DPAC** originated solely from the MR-TADF dopant, with slightly broadened FWHMs of 48 nm and similar Commission International de l'Éclairage (CIE) coordinates of (0.14, 0.54) and (0.14, 0.56) (Fig. 4C). The EQE_{max}s, achieved at 1% doping ratio were 21.1% and 28.2% for **BN-DMAC** and **BN-DPAC**, respectively, in consistency with the Φ_{PL} of each emitter in doped film with same guest concentration if assuming an outcoupling efficiency (η_{out}) at 30%. Noticeably, the efficiency roll-off was significantly alleviated in the case of **BN-DPAC**, with EQEs maintaining as high as 27.7% under brightness of 100 cd m^{-2} (for displays) and 19.4% under 1000 cd m^{-2} (for lighting applications). The decent roll-off characteristics of **BN-DPAC** was partially ascribing to its faster triplet upconversion,

and more importantly the effective suppression of bimolecular interactions and notorious triplet-exciton involved quenching process by the shielding phenyl moieties. Fitting of EQE-*J* curves supported the significant role of triplet-triplet annihilation (TTA) in efficiency roll-off mechanism, with higher critical current density (J_0) for **BN-DPAC**-based device comparing to the **BN-DMAC** counterpart (Fig. S3).

Encouraged by the promising results, the doping ratio of **BN-DPAC** was furtherly optimized in the same device architecture (Fig. S4). A significant bathochromic shift of the EL curves from 504 nm to 516 nm was noticed at increased doping concentration from 1 wt% to 5 wt%, leading to much improved green color purity as indicated by the CIE coordinate of (0.21, 0.65) closed to the National Television System Committee (NTSC) standard green-light CIE coordinate of (0.21, 0.71), despite a moderate decline of EQE_{max} to 23.5% possibly caused by the slightly imbalanced charge-carrier transfer referring to the *J-V-L* profile. Further increasing of the doping concentration to 10 wt% could still maintain a EQE_{max} value of 21.4%, but marginally changed the spectral profiles. In all cases, the device efficiency remained stable at practical high luminance, thanks to the steric effect at molecular edge. Noteworthily, the **BN-DPAC**-based devices, including the narrow EL emission, remarkable EQE and efficiency roll-off character, were among the best overall performances of green OLEDs.

In a nutshell, a unique non-planar **BN-AC** skeleton was proposed to derivatize two green MR-TADF emitters featuring decent quantum yields and color purity. Due to the synergistic effects of rigid backbone and loose intermolecular interactions that could minimize non-radiative energy loss from vibration and bimolecular quenching process,

the corresponding devices displayed appealing performances, with simultaneously narrowband emission and state-of-the-art EQE values up to 28.2% without utilizing any assistant dopant. Installation of more bulky dangling substituents was proved effective to alleviate the roll-off behavior, as witnessed by an efficiency drop of only 1.8% at 100 cd m^{-2} for **BN-DPAC**-based device. Increasing of dopant concentration redshifted the EL signal into pure green region with CIE coordinates of (0.21, 0.65) while maintaining a high efficiency. The results would shed light on the design of more advanced MR-TADF-based OLEDs.

Declaration of Competing Interest

The authors declare no competing financial interests or personal relationships that could have appeared to influence the work reported in this paper.

Acknowledgements

This research is financially supported by the National Natural Science Foundation of China (51903159, 91833304), the Shenzhen Science and Technology Program (KQTD20170330110107046, JCYJ20190808151209557), the China Postdoctoral Science Foundation (2020M682852, 2019M663065), the Natural Science Foundation of Shenzhen University (2019001), and the Foundation for Basic and Applied Research of Guangdong Province (2019A1515110915). We thank the Instrumental Analysis Center of Shenzhen University for analytical support.

References

[1] L.-S. Cui, A. J. Gillett, S.-F. Zhang, H. Ye, Y. Liu, X.-K. Chen, Z.-S. Lin, E. W. Evans, W. K. Myers, T. K. Ronson, H. Nakanotani, S. Reineke, J.-L. Bredas, C. Adachi, R. H. Friend, *Nat. Photon.* **2020**, *14*, 636-642.

[2] Q. Zhang, B. Li, S. Huang, H. Nomura, H. Tanaka, C. Adachi, *Nat. Photon.* **2014**, *8*, 326-332.

[3] H. Uoyama, K. Goushi, K. Shizu, H. Nomura, C. Adachi, *Nature* **2012**, *492*, 234-238.

[4] C.-C. Peng, S.-Y. Yang, H.-C. Li, G.-H. Xie, L.-S. Cui, S.-N. Zou, C. Poriel, Z.-Q. Jiang, L.-S. Liao, *Adv. Mater.* **2020**, 2003885.

[5] Z. Yang, Z. Mao, Z. Xie, Y. Zhang, S. Liu, J. Zhao, J. Xu, Z. Chi, M. P. Aldred, *Chem. Soc. Rev.* **2017**, *46*, 915-1016.

[6] P. L. dos Santos, J. S. Ward, D. G. Congrave, A. S. Batsanov, J. Eng, J. E. Stacey, T. J. Penfold, A. P. Monkman, M. R. Bryce, *Adv. Sci.* **2018**, *5*, 1700989.

[7] J. Huang, H. Nie, J. Zeng, Z. Zhuang, S. Gan, Y. Cai, J. Guo, S.-J. Su, Z. Zhao, B. Z. Tang, *Angew. Chem. Int. Ed.* **2017**, *56*, 12971-12976.

[8] S.-J. Zou, F.-M. Xie, M. Xie, Y.-Q. Li, T. Cheng, X.-H. Zhang, C.-S. Lee, J.-X. Tang, *Adv. Sci.* **2020**, *7*, 1902508.

[9] D. Hall, S. M. Suresh, P. L. dos Santos, E. Duda, S. Bagnich, A. Pershin, P. Rajamalli, D. B. Cordes, A. M. Z. Slawin, D. Beljonne, A. Köhler, I. D. W. Samuel, Y. Olivier, E. Zysman-Colman, *Adv. Optical Mater.* **2020**, *8*, 1901627.

[10] Y. Yuan, X. Tang, X.-Y. Du, Y. Hu, Y.-J. Yu, Z.-Q. Jiang, L.-S. Liao, S.-T. Lee, *Adv. Optical Mater.* **2019**, *7*, 1801536.

[11] X. Li, Y.-Z. Shi, K. Wang, M. Zhang, C.-J. Zheng, D.-M. Sun, G.-L. Dai, X.-C. Fan, D.-Q. Wang, W. Liu, Y.-Q. Li, J. Yu, X.-M. Ou, C. Adachi, X.-H. Zhang, *ACS Appl. Mater. Interfaces* **2019**, *11*, 13472-13480.

[12] D. Sun, S. M. Suresh, D. Hall, M. Zhang, C. Si, D. B. Cordes, A. M. Z. Slawin, Y. Olivier, X. Zhang, E. Zysman-Colman, *Mater. Chem. Front.* **2020**, *4*, 2018-2022.

[13] H. L. Lee, W. J. Chung, J. Y. Lee, *Small* **2020**, *16*, 1907569.

[14] H. Lim, H. J. Cheon, S.-J. Woo, S.-K. Kwon, Y.-H. Kim, J.-J. Kim, *Adv. Mater.* **2020**, *32*, 2004083.

[15] J.-M. Teng, Y.-F. Wang, C.-F. Chen, *J. Mater. Chem. C* **2020**, *8*, 11340-11353.

[16] T. Hatakeyama, K. Shiren, K. Nakajima, S. Nomura, S. Nakatsuka, K. Kinoshita, J. Ni, Y. Ono, T. Ikuta, *Adv. Mater.* **2016**, *28*, 2777-2781.

[17] S. Oda, B. Kawakami, R. Kawasumi, R. Okita, T. Hatakeyama, *Org. Lett.* **2019**, *21*, 9311-9314.

[18] N. Ikeda, S. Oda, R. Matsumoto, M. Yoshioka, D. Fukushima, K. Yoshiura, N. Yasuda, T. Hatakeyama, *Adv. Mater.* **2020**, *32*, 2004072.

[19] K. Matsui, S. Oda, K. Yoshiura, K. Nakajima, N. Yasuda, T. Hatakeyama, *J. Am. Chem. Soc.* **2018**, *140*, 1195-1198.

[20] S. Nakatsuka, H. Gotoh, K. Kinoshita, N. Yasuda, T. Hatakeyama, *Angew. Chem. Int. Ed.* **2017**, *56*, 5087-5090.

[21] H. Hirai, K. Nakajima, S. Nakatsuka, K. Shiren, J. Ni, S. Nomura, T. Ikuta, T. Hatakeyama, *Angew. Chem. Int. Ed.* **2015**, *54*, 13581-13585.
[22] S. Madayanad Suresh, D. Hall, D. Beljonne, Y. Olivier, E. Zysman-Colman, *Adv. Funct. Mater.* **2020**, *30*, 1908677.
[23] Y. Kondo, K. Yoshiura, S. Kitera, H. Nishi, S. Oda, H. Gotoh, Y. Sasada, M. Yanai, T. Hatakeyama, *Nat. Photon.* **2019**, *13*, 678-682.
[24] Y. Xu, Z. Cheng, Z. Li, B. Liang, J. Wang, J. Wei, Z. Zhang, Y. Wang, *Adv. Optical Mater.* **2020**, *8*, 1902142.
[25] Y. Zhang, D. Zhang, J. Wei, Z. Liu, Y. Lu, L. Duan, *Angew. Chem. Int. Ed.* **2019**, *58*, 16912-16917.
[26] Y. Xu, C. Li, Z. Li, Q. Wang, X. Cai, J. Wei, Y. Wang, *Angew. Chem. Int. Ed.* **2020**, *59*, 17442-17446.
[27] Y. Zhang, D. Zhang, J. Wei, X. Hong, Y. Lu, D. Hu, G. Li, Z. Liu, Y. Chen, L. Duan, *Angew. Chem. Int. Ed.* **2020**, *59*, 17499-17503.
[28] M. Yang, I. S. Park, T. Yasuda, *J. Am. Chem. Soc.* **2020**, *142*, 19468-19472.
[29] D. Zhang, X. Song, A. J. Gillett, B. H. Drummond, S. T. E. Jones, G. Li, H. He, M. Cai, D. Credgington, L. Duan, *Adv. Mater.* **2020**, *32*, 1908355.
[30] S. H. Han, J. H. Jeong, J. W. Yoo, J. Y. Lee, *J. Mater. Chem. C* **2019**, *7*, 3082-3089.
[31] K. H. Lee, J. Y. Lee, *J. Mater. Chem. C* **2019**, *7*, 8562-8568.
[32] S. S. Kothavale, J. Y. Lee, *Adv. Optical Mater.* **2020**, *8*, 2000922.
[33] X. Gong, P. Li, Y.-H. Huang, C.-Y. Wang, C.-H. Lu, W.-K. Lee, C. Zhong, Z. Chen, W. Ning, C.-C. Wu, S. Gong, C. Yang, *Adv. Funct. Mater.* **2020**, *30*, 1908839.
[34] J. Lee, N. Aizawa, M. Numata, C. Adachi, T. Yasuda, *Adv. Mater.* **2017**, *29*, 1604856.
[35] W. Li, B. Li, X. Cai, L. Gan, Z. Xu, W. Li, K. Liu, D. Chen, S.-J. Su, *Angew. Chem. Int. Ed.* **2019**, *58*, 11301-11305.